Shorted Patch Antenna With Multi Slots for a UHF RFID Tag Attached to a Metallic Object

MINH-TAN NGUYEN[1,2], YI-FANG LIN[1], CHIEN-HUNG CHEN[3], (Member, IEEE), CHUN-HSIEN CHANG[1], AND HUA-MING CHEN[1], (Senior Member, IEEE)

[1]Institute of Photonics Engineering, National Kaohsiung University of Science and Technology, Kaohsiung 80778, Taiwan
[2]Institute of Research and Applied Technological Science, Dong Nai Technology University, Biên Hòa, Dong Nai 76000, Vietnam
[3]Department of Avionics Engineering, R.O.C. Air Force Academy, Kaohsiung 82047, Taiwan

Corresponding author: Hua-Ming Chen (hmchen@nkust.edu.tw)

ABSTRACT This study developed a miniature tag antenna attached to a backing metal for ultrahigh-frequency radio frequency identification (RFID) applications. The impedance of this antenna can be easily controlled at the desired fixed frequency by using different mechanisms and was not considerably affected by backing metal size. This antenna comprises a radiating patch with double I-shaped slots and a ground layer shorted to a narrow inductive plate. Loading a closed slot in the center of the patch and the open slits enabled flexible frequency tuning to match the complex impedance of the microchip used. This tag antenna has a low profile of $28.02 \times 25.02 \times 2.61$ mm^3 ($0.086 \times 0.076 \times 0.0079$ λ_0^3), and it provides a high power transmission coefficient of 99.74%, realized gain of -2.3 dB, and a reading distance of 8.1 m when it is located at the center of a metallic plate of size 250×250 mm^2. The operational frequency of the proposed antenna was designed to reside the frequency bands for North and South America (860–960 and 902–928 MHz, respectively). Measurements of the antenna prototype proved that the experimental results agreed with the simulated data.

INDEX TERMS Metallic tag antenna, shorted inductive plate, reading distance, RFID tag, I-shaped patch.

I. INTRODUCTION

The manufacturing cost of radio frequency identification chips has decreased greatly owing to rapid developments in semiconductor technology. In particular, smaller RFID chips with lower power consumption, greater memory capacity, faster signal processing, wider design choices, and more secure data transmission are now easily available [1]. RFID devices are extensively used for applications such as toll roads, sensing systems, object tracking, supply chain management, and security systems [2], [3]. Generally, in a practical passive RFID system, each individual object is assembled with a small and low-cost tag. A tag includes an antenna designed by users, and it can operate in various frequency bands. The behavior of an ideal RFID system is unaffected by factors such as orientation, environment, and the presence of the object on which the tag is placed [4]. Nonetheless, as a tag antenna is usually located on or near a metallic object, the properties of this object strongly influence the operational effectiveness and principal parameters of the antenna, such as

the input impedance, radiation efficiency, power transmission coefficient, total gain, and radiation angular pattern sensitivity [5], [6]. Several studies have suggested methods to solve these problems and to improve tag antenna performance. In [7]–[10], tags based on an artificial magnetic conductor (AMC) surface have been proposed to improve tag gain and radiation patterns. These antennas were designed with a bowtie-shaped or modified dipole structure on the top and AMC unit cells inserted in the inner layers or the backplane as a ground plane on the bottom. However, such designs complicate the structure of AMC tag antennas and greatly increase their profile even though it is beneficial to insulate the antenna from the effects of the backing metal [11]. Consequently, these tag antennas are not compact or cost effective. To reduce tag size, planar inverted-F antenna (PIFA) structures have been recommended [12].

A PIFA was developed as a platform-tolerant design to reduce the size of tag antennas [13]. The utilized microchip's impedance is commonly configured to a very high Q factor to improve its sensitivity. The input impedance is sensitive to small changes in frequency with a high Q value, and this makes it difficult to perform conjugate impedance matching

The associate editor coordinating the review of this manuscript and approving it for publication was Hussein Attia.

for the designed antennas [14], [15]. In particular, some studies [16], [17] have proposed antenna structures with greatly improved impedance matching and reduced size by embedding a slotted via-patch and a conductive solution in the middle layer; however, the low radiation efficiency of these designs greatly affects the achievable reading distance of the tag antenna. Additionally, the input impedance adjustment of tag antennas is difficult. Electrically small antennas with loaded via-patches and shorting stubs have been proposed to achieve high radiation efficiency [18]–[20]. However, these designs require parameter configuration between the feed point, feed radiators, and via-holes, which is difficult to perform optimally through measurements. Moreover, applying multiple vias or via-patches for the short circuit affects the achievable efficiency if the antenna structure is not configured appropriately during fabrication. Therefore, the fine-tuning process is relatively demanding, and manufacturing costs can rise substantially.

Recent design advances with the folded-patch technique have enhanced the performance and reduced the size of tags [21], [22]. Studies have miniaturized tag antennas by using multiple shorting stubs in the center and a vertex on the top patch to form inner or ground layers [23] and [24]. However, the combination of multiple shorting stubs and meandered slot lines in the tag structure resulted in poor impedance matching between the antenna and the microchip; this, in turn, reduced the power transmission coefficient to less than 0.7 and the achievable reading range to less than 5 m. Another study [25] significantly improved the power transmission coefficient to approximately 99.7% and achieved a large read distance of at least 7 m. However, similar designs have been described in [21]–[24]. Further, these tags required more ground planes or inner radiating planes; this complicated the structure and increased the total size of the tag antennas. In addition, the folded-patch technique required a complex fabrication procedure and made tuning difficult.

This study developed an electrically small tag antenna structure attached to a backing metal object with flexible impedance matching between the antenna and the IC chip. The proposed antenna was designed with a compact and low-cost structure, and it did not require multiple vias for the short circuit, extra ground layers, or inner radiation layers. Further, its fabrication procedure was simple and did not require the complicated techniques and multilayer structures of previously proposed antennas [21]–[25]. In addition, the proposed antenna structure could be adjusted easily through the coarse tuning of the width of the shorted inductive plate, I-slot 1, and open and closed slots of the I-shaped patch. Fine-tuning the length of I-slot 2 and creating two open slits achieved conjugated matching with the input impedance of the UCODE8/8m chip, which is the newest microchip version of the UCODE family developed by NXP. The UCODE8/8m chip has high performance and is suitable for use in demanding RFID tagging applications. The effectiveness of the proposed tag, including the return loss (S_{11}), realized gain (G_r), power transmission coefficient (τ), and maximum read range (R_{max})
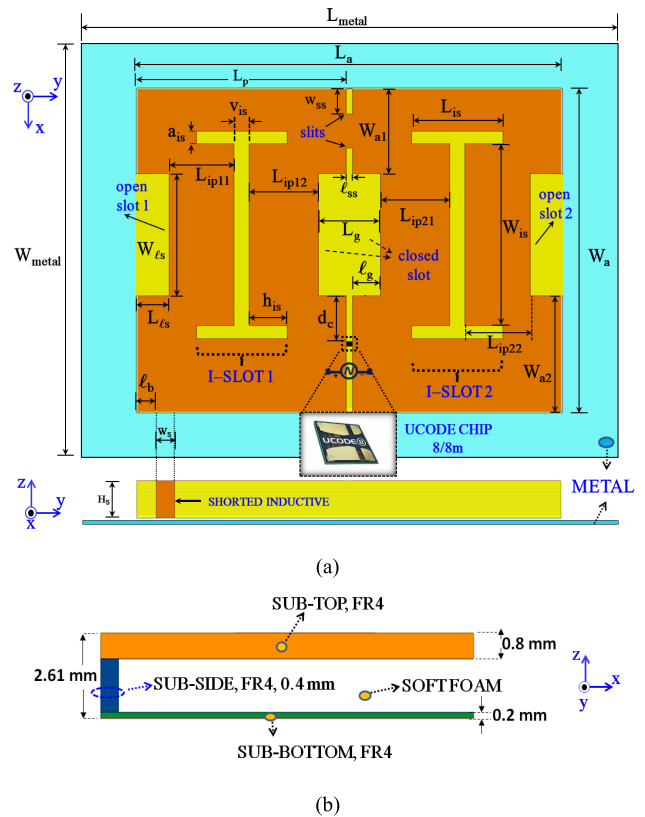

FIGURE 1. Two layers structure of the proposed antenna supported by the soft foam with the backing metal plate. (a) Top view and shorted inductive plate; (b) Side view of FR4 substrates.

of the proposed antenna fixed at the center of a metal object with a size of 250×250 mm^2 was investigated. All simulation results were implemented using ANSYS HFSS Electromagnetics 2019 [26].

The remainder of this paper is organized as follows. Section II describes the design layout and optimization of the proposed structure. Section III describes the design analysis and surface current distribution. Section IV discusses the effects of the antenna's parameters and different sizes of backing metal plates. Section V details the parameter measurements and compares the proposed antenna with those reported previously.

II. ANTENNA CONFIGURATION AND OPTIMIZATION

The shorted inductive double I-shaped patch antenna with two embedded I-slots attached to the metallic object (Fig. 1a) was designed and fabricated for the operational frequency ranges for North and South America (860–960 and 902–928 MHz, respectively). A small space of 0.1 mm existed between the tag and the backing metal, and the tag was fixed to the center of a metallic plate (size: 250×250 mm^2). The proposed structure included a double I-shaped radiating patch that was shorted to the ground layer by using a thin inductive plate of width W_s placed at the long side of the patch. Both layers were printed on the FR4 substrates with

TABLE 1. The optimal antenna configuration parameters.

Parameters	Values (mm)	Parameters	Values (mm)	Parameters	Values (mm)
W_{metal}	250	W_{ls}	9.4	h_{is}	2.5
L_{metal}	250	L_{ls}	2.1	w_{ss}	2.0
W_a	25.02	l_b	1.3	l_{ss}	0.7
L_a	28.02	L_{ip11}	4.3	L_g	4.1
L_p	13.65	L_{ip12}	4.35	l_g	1.7
a_{is}	1.0	L_{ip21}	4.6	d_c	3.0
v_{is}	1.0	L_{ip22}	4.45	W_{a1}	6.6
L_{is}	6.0	w_s	1.2	W_{a2}	9.0
W_{is}	14	H_s	2.61		

FIGURE 2. The prototype dimensions of the proposed antenna in top view (1), bottom view (2) and side view (3).

a relative permittivity of 4.3, dielectric loss tangent of 0.02, and individual thickness of 0.8 mm and 0.2 mm [27]. The dimensions of the thin shorted inductive plate on the side of the antenna were $W_s \times 2.61$ mm^2. The antenna was also etched on a single-sided FR4 substrate with a thickness of 0.4 mm (Fig. 1b). A narrow gap of 0.5 mm was etched at the center of the patch, and an RFID chip was attached in between. The space between the radiating plate and the ground plate was reinforced by rectangular polyethylene foam (PP2) with a volume of $28.02 \times 24.62 \times 1.61$ mm^3, a dielectric constant of $\varepsilon_r = 1.03$ (nearly equal to that of the air substrate), and a loss tangent of $\tan \delta = 0.0001$ [28]. I-slot 1 and I-slot 2 were symmetrically etched on I-shaped slots with a size of $L_{is} \times 16$ mm to form a parallel structure that helped control the resonance frequency. Two opposite open slits were formed with gaps of $0.7 \times W_{ss}$ mm^2 to slowly reduce the resonance frequency. Further, this design was focused on flexible impedance matching methods; therefore, coarse tuning was initially performed by changing the parameters of the shorted inductive plate, I-slot 1, as well as open and closed slots. Then, fine-tuning was performed by varying the size of I-slot 2 and two open slits to realize perfect impedance matching between the tag and the RFID microchip. The UCODE8/8m microchip was used in the simulation calculation and measurement; its input excitation port has an impedance of $13-j191$ Ω, a minimum threshold power of -22.9 dBm (READ conditions), and a minimum sensitivity of -17.8 dBm (WRITE conditions) at an operation frequency of 915 MHz (these initial parameters were obtained from the manufacturers' datasheet). A crucial consideration based on the datasheet of the UCODE 8/8m chip it that multiple input impedance values can be chosen for designing an appropriate antenna structure. However, to optimize the design, an input impedance of $15-j217$ Ω was chosen for the microchip (the actual measured impedance of the chip is described in the next section). The chip was also configured with a single-slit assembly to enable easier fabrication; this enabled the manufacture of short-circuiting RF1 (antenna connector 1) with a TP1 pad and RF2 (antenna connector 2) with a TP2 pad [29]. Fig. 1a shows the main parameter variables of the proposed antenna, and Table 1 list their optimized values. Furthermore, Fig. 2 presents photographs of the proposed antenna prototype.
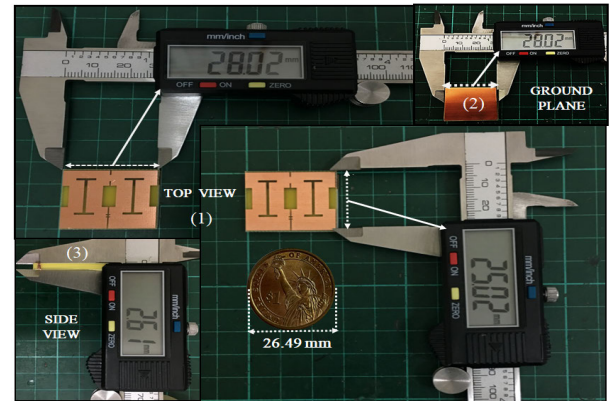
III. INPUT IMPDEDANCE MEASUREMENT OF RFID CHIP

The complex impedance ($Z_{Chip} = R-jX_C$) varies with the RFID chip's frequency and strongly influences the behavior of the tag antenna. Therefore, the input impedance of an RFID chip should be measured before the tag antenna is designed [30], [31]. This was done using a measurement probe with a vector network analyzer (VNA) having a frequency range of 800–1000 MHz. The balun was supported by EZ-Probe through a coaxial cable to determine the minimum input power sensitivity and the input resistance and reactance of the UCODE8/8m by observing the corresponding fixed marker on the Smith chart (see Fig. 3a). Furthermore, the probe was calibrated through the application of a TDR calibration substrate with open, short, and loads before the determination of whether the pointer position deviated from the established standard (see Figs. 3a and 3b).

The measurement calibration greatly affected the input impedance of the antenna and microchip. Therefore, the balun probe calibration process was used; its steps are described below:

Step 1: The TDR calibration substrate was renoved from the VNA, as shown in Fig. 3b. The balun was untouched for all circuit models on the TDR.

Step 2: The balun probe was sequential touched the short circuit and open circuit models on the calibration substrate.

Step 3: The balun probe was touched two pads of a copper piece, which was set to equivalent loads of 28 Ω, 50 Ω, or 75 Ω on the calibration substrate. The reflection coefficient at 840–960 MHz would reach below -10 dB.

To obtain the input impedance of the UCODE8/8m chip, the following measurement process was introduced. First, the calibrated balun probe was fixed at the pads of the chip to identify the minimum read sensitivity, which was almost -21.9 dBm around the operational frequency (see Fig. 4).

Then, the changes in the resistance and reactance of the chip as a function of the frequency range (800–1000 MHz) were determined, as shown in Fig. 5. Figs. 4 and 5 show that the best measured input impedance and sensitivity at 915 MHz were $15-j217$ Ω and -21.9 dBm, respectively. A
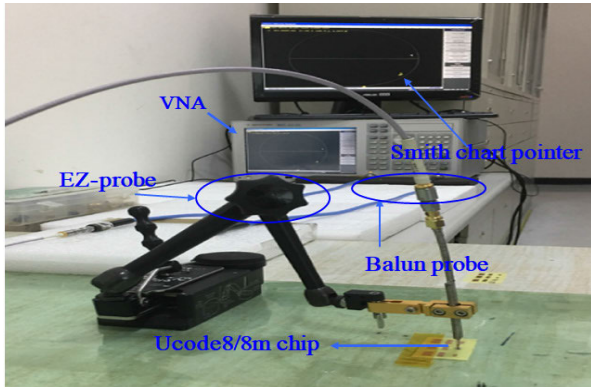
(a)
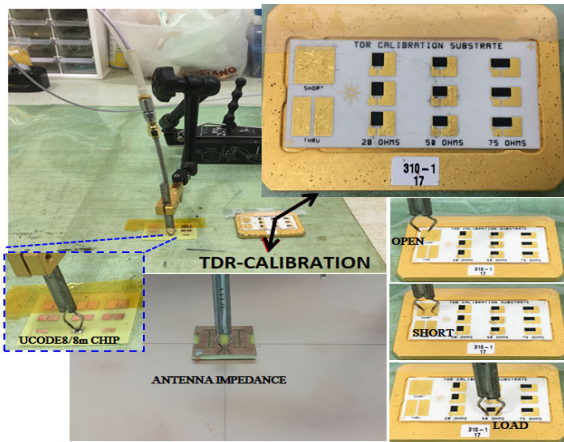
(b)

FIGURE 3. (a) The chip impedance measurement set; (b) TDR calibration substrate.
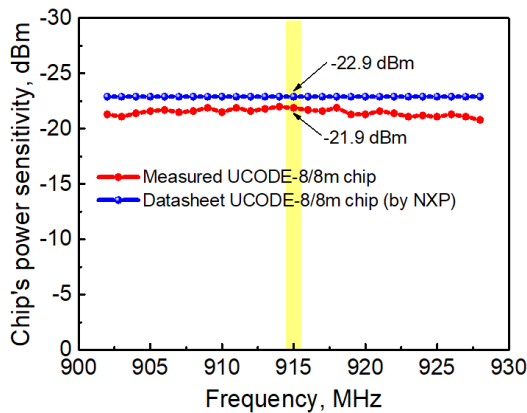

FIGURE 4. The measured threshold power sensitivity of UCODE 8/8m chip across the different frequencies.

slight deviation was seen between the measurement results and the UCODE 8/8m chip manufacturer's datasheet. This discrepancy arose from the deformation of the strap structure (Fig. 3b) when the flexible pins of the balun probe were attached to two pads of the strap soldered to the chip's pins
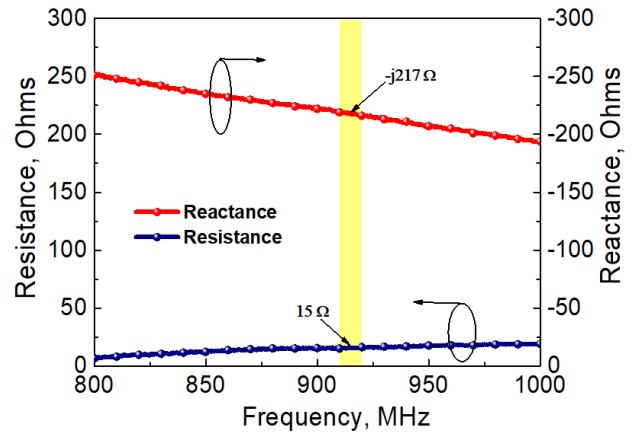

FIGURE 5. The changes of the chip's impedance across the different frequencies.

during the measurement process. Further, the manufacturing tolerances of the active devices caused the resistance and reactance to vary [32]–[34]. Therefore, the measured input impedance of 15-j217 Ω was used in all design analyses and calculations described in the next section.

IV. DESIGN ANALYSIS AND SURFACE CURRENT DISTRIBUTION

Two fundamental considerations that markedly influence the effectiveness of the structure of an electrically small antenna are the antenna's radiation efficiency and the conjugated impedance matching between the antenna and the microchip. The main parameters of the chip were determined as described in Section III for a resonance frequency of 915 MHz and input complex impedance of 15-j217 Ω. This indicated that the tag antenna should be designed to achieve a tradeoff among impedance matching, reasonable radiation efficiency, and antenna size when the antenna is mounted at the center of a metallic plate of size 250 × 250 mm². The design method is described as follows:

Phase 1: The I-shaped radiating plane with I-slot 1 in the middle of the antenna does not include a shorted inductive plate in the first stage of the design. Fig. 6a shows that the resonance frequency is much higher than that desired for the proposed antenna; this design structure resulted in a resistance of 15 Ω and reactance of j217 Ω at 1250 MHz, and the antenna had very low radiation efficiency and low gain, as shown in Fig. 6b.

Phase 2: To lower the tag antenna's resonance frequency and improve the radiation efficiency, a small inductive plate with width of W_S = 1.2 mm was used to short the I-shaped resonator on the top and ground planes, as shown in Fig. 7a. Upon the application of the shorted inductive plate, the resonance frequency of the tag antenna was observed to become significantly lower with an input impedance of 15+j217 Ω at 950 MHz, and the total gain was approximately −4.1 dB, as shown in Fig. 7b. Notably, the tag's resonance frequency was sensitive to small changes in the sizes of the shorted
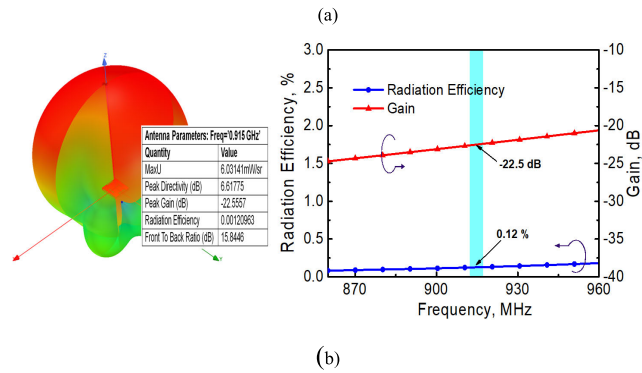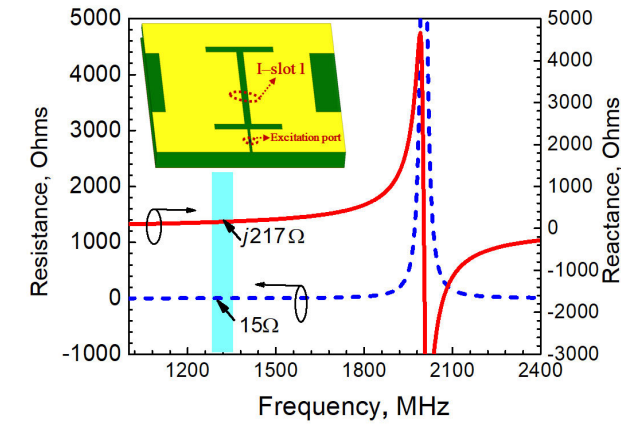
FIGURE 6. The simulated structure of the proposed antenna for the case not having a shorted inductive, I-patch 1, I-slot 2 and slits. (a) Resistance and reactance. (b) The total gain in 3D & 2D.
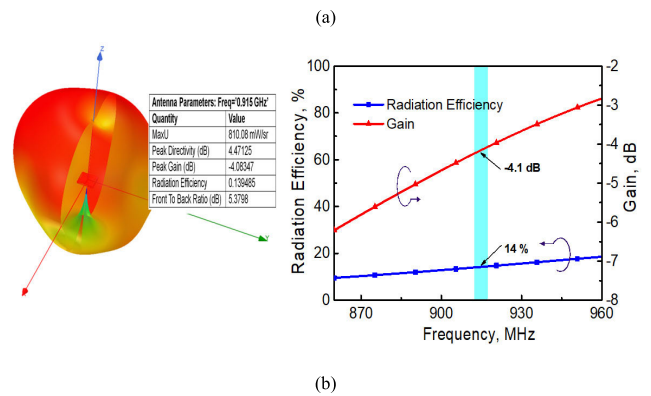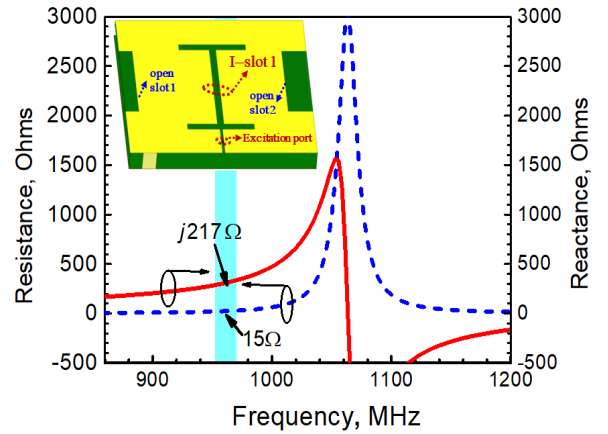

FIGURE 7. The simulated structure of the proposed antenna for the case not having I-patch 1, I-slot 2 and slits. (a) Resistance and reactance. (b) The total gain in 3D & 2D.

inductive plate and open and closed slots. Therefore, both the changes were used for coarse tuning in the optimization processes (further analysis in Section V).

Phase 3: The radiation efficiency and lower shifting resonance frequency greatly increased because of the extension of the surface current distribution density on the I-shaped patch resonator. Consequently, the second I-shaped patch was combined with the first I-shaped patch to form two opposite open slits with dimensions of 0.7×2 mm². As a result, the radiation efficiency increased by approximately 19.7 %, and the resonance frequency decreased and became close to the desired frequency of 925 MHz, as shown in Figs. 8a and 8b.

Phase 4: Finally, to achieve the complex impedance matching of the microchip, the resonance frequency of the proposed antenna was shifted toward the desired value; this also optimized the radiation efficiency or gain. I-slot 2 was produced in the center of I-patch 2. The presence of I-slot 2 further increased the length of current paths and caused the tag antenna to become more inductive, thereby reducing its resonance frequency to 915 MHz (see Fig. 9a). Further, Pfeiffer [35] found that the radiation efficiency of a small antenna depends on the surface resistivity of the metal, which depends on the operating frequency and conductivity and can be approximated as follows:

$$ka \sim (k\delta_s)^{1/4} = (2\omega\varepsilon_0/\sigma)^{1/8} \qquad (1)$$

where k is the wave number ($2\pi/\lambda$), a is the effective radius of nonspherical antennas and is assumed to be expressed as $a = (3V/(4\pi))^{1/3}$, where V is the antenna volume, and σ is the conductivity of the antenna.

From this equation, when $ka \approx 0.08$ for the proposed antenna, that will result in a radiation efficiency of 23%. Therefore, after the insertion of I-slot 2 into I-shaped patch 2, the achievable radiation efficiency and gain were approximately 22.1 % and -1.8 dB, respectively (see Fig. 9b); these are reasonable results for an electrically small tag [21].

Fig. 9c shows the surface current distribution density of the proposed antenna attached to a metallic plate of size 250×250 mm² and the resonant current directions on both radiating I-shaped patches at 915 MHz. The surface current was distributed asymmetrically between the two I-shaped patches. This implies that the high current densities were focused on the shorted inductive plate, I-slot 1, as well as the open and closed slots, suggesting that those structures are useful for the coarse tuning of the resonance frequency of the tag antenna. However, the lower current densities were concentrated around I-slot 2 and a slit, indicating that will effectively match the impedance of the microchip upon fine-tuning the proposed antenna, as shown in Section V. The antenna size was fixed at $28.02 \times 25.02 \times 2.61$ mm³ in all designs.
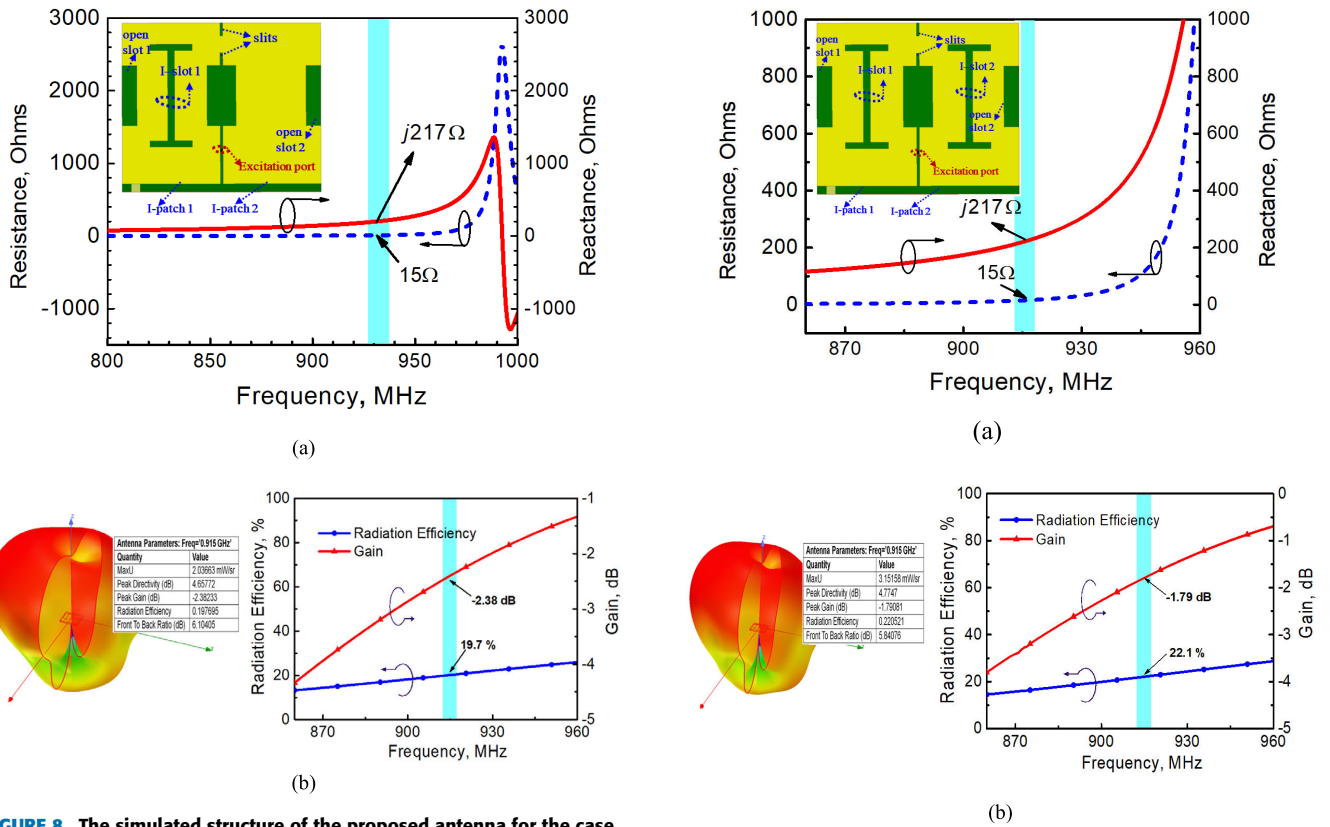
(a)

(b)

FIGURE 8. The simulated structure of the proposed antenna for the case not having I-slot 2. (a) Resistance and reactance. (b) The total gain in 3D & 2D.

V. PARAMETERS EVALUATION

The proposed antenna's characteristics, including the input impedance, reflection coefficient, power transmission coefficient, radiation efficiency, and gain, were evaluated to consider the impact of the primary properties on the performance of the tag. The fundamental variables of the proposed antenna include the total length of the open and closed slots ($L_{IP} = L_{ip11} + L_{ip12} + L_{ip21} + L_{ip22}$), the width of the shorted inductive (W_s), the size of two slits (W_{ss}), and the total lengths of I-slot 1 ($L_{IS1} = 2L_{is} + V_{is}$) and I-slot 2 ($L_{IS2} = 2L_{is} + V_{is}$). For all evaluation cases, the proposed antenna was fixed at the middle of a metallic plate of size 250 × 250 mm^2 with a small open space of 0.1 mm. The aim of this study was to design a flexible and miniaturized tag structure whose conjugate impedance could be easily matched to that of a microchip through the modification of several parameter variables. The effects of the open and closed slots were first observed (Fig. 10). Fig. 10b shows the reflection coefficient; the tag's resonance frequency was fairly sensitive to the length of the open and closed slots. The tag's desirable frequency was greatly shifted at a rate of 17.5 MHz upon the variation of several variables (L_{ip11}, L_{ip12}, L_{ip21}, L_{ip22}) and the maintenance of total L_{IP} in every increment of 1.6 mm. This is because the tag's resistance and reactance increased when the L_{IP} of the open and closed slots decreased (Fig. 10a). The obtained impedance bandwidth for a 3-dB
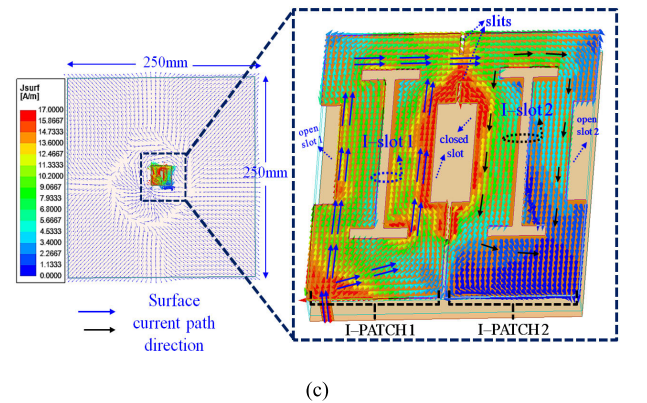

(a)

(b)

(c)

FIGURE 9. The simulated structure of the proposed antenna with a shorted inductive, I-patch 1, I-slot 1, I-patch 2, I-slot 2, and slits; (a) resistance and reactance. (b) The total gain in 3D & 2D. (c) The surface current distribution.

axial ratio greater than 1.85% ranged from 907 to 924 MHz. As shown in Fig. 10c, for different values of L_{IP}(16.1 mm, 17.7 mm, and 19.3 mm), optimal matching (approximately 100%) was achieved in the power transmission coefficient between the antenna and the microchip at the frequencies 890 MHz, 915 MHz, and 935 MHz.
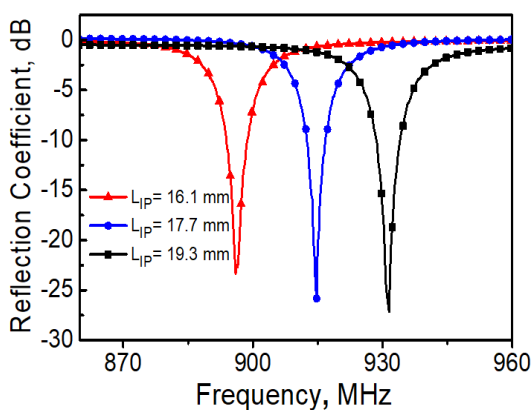
Next, the important parameters of I-slot 1 ($L_{IS1} = 2L_{is} + V_{is}$) were considered. Fig. 11a shows that the resistive and inductive parameters greatly increased every 1.5 mm as the length of the open and closed slots decreased in L_{IS1}; consequently, the level and the position of the resonance frequency
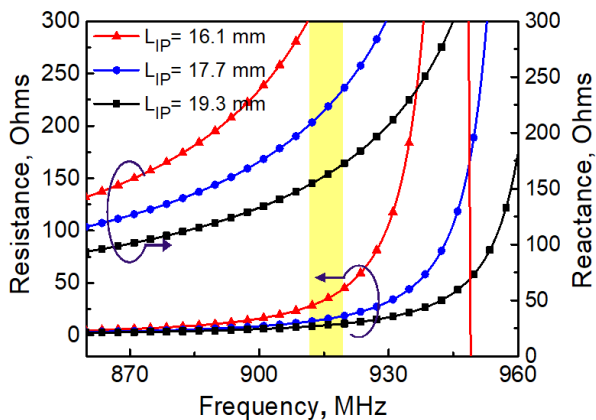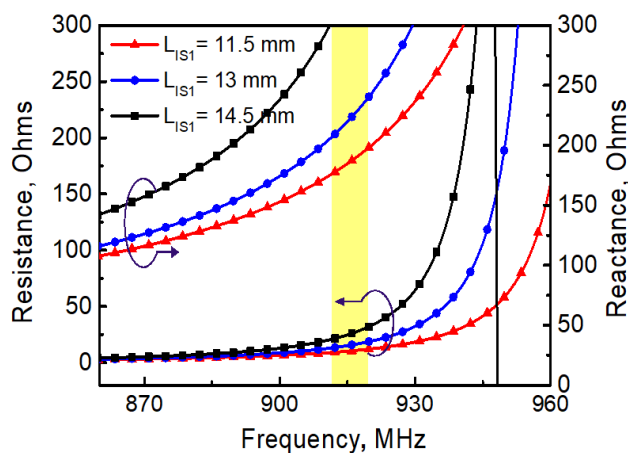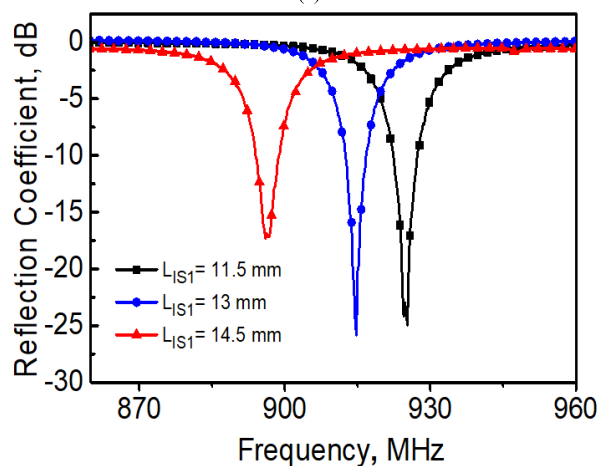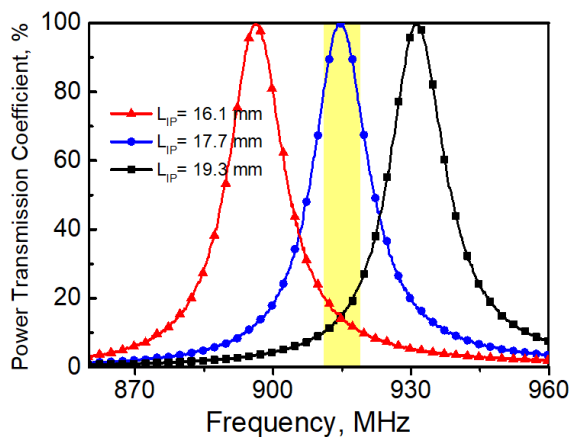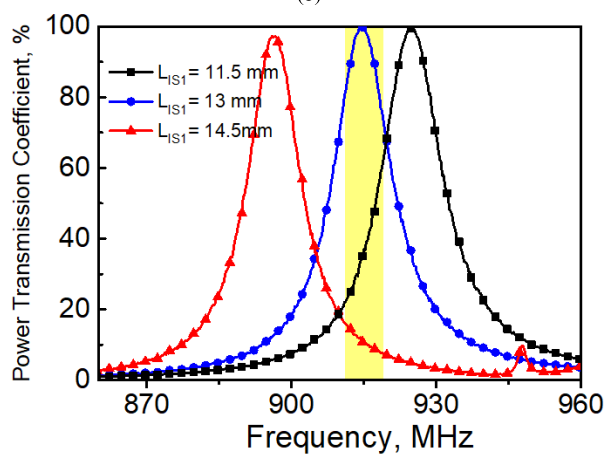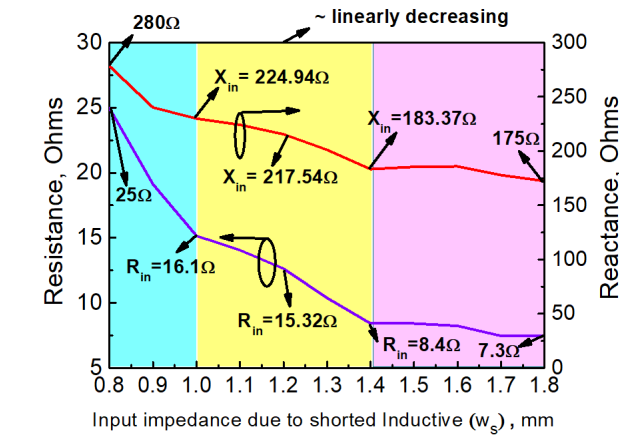
FIGURE 10. The impact on the open and closed slots ($L_{IP} = L_{ip11} + L_{ip12} + L_{ip21} + L_{ip22}$) to (a) The input impedance. (b) Reflection coefficient (dB). (c) Power transmission coefficient of the proposed antenna across the different frequencies.

FIGURE 11. The impact on I-slot 1 ($L_{IS1} = 2L_{is} + V_{is}$) to (a) The input impedance. (b) Reflection coefficient (dB). (c) Power transmission coefficient across the different frequencies.

decrease rapidly by increasing the values of L_{IS1} from 13 to 14.5 mm, as shown in Fig. 11b. Besides, as the length of L_{IS1} increase gradually from 11.5 to 13 mm the level of the resonant reflection coefficients remained almost stable at -26 dB

with a slow shifting for the lower frequency side. Therefore, the power transmission coefficients remained around 100% when the resonance frequency became greater than or equal to 915 MHz, as shown in Fig. 11c.

(a)

(b)

(a)

(b)

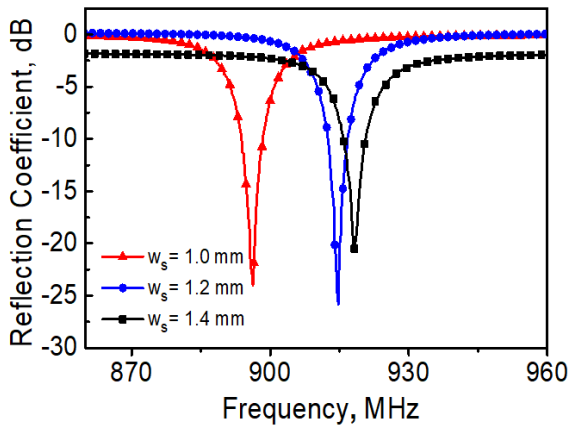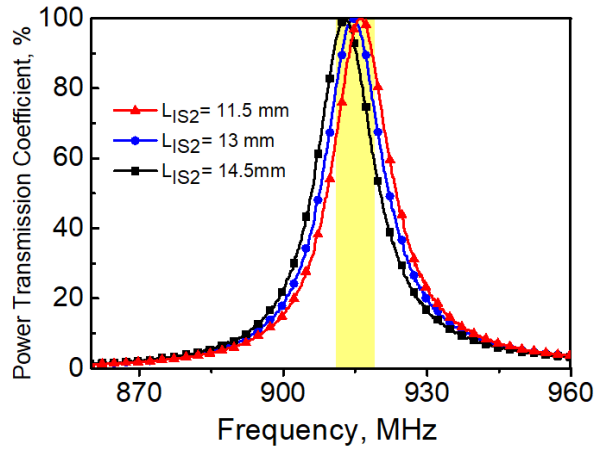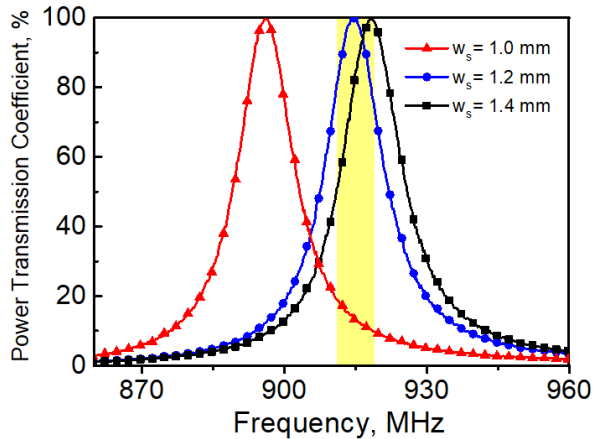**FIGURE 13.** The impact on I-slot 2 ($L_{IS2} = 2L_{is} + V_{is}$) to (a) The input impedance. (b) Power transmission coefficient across the different frequencies.
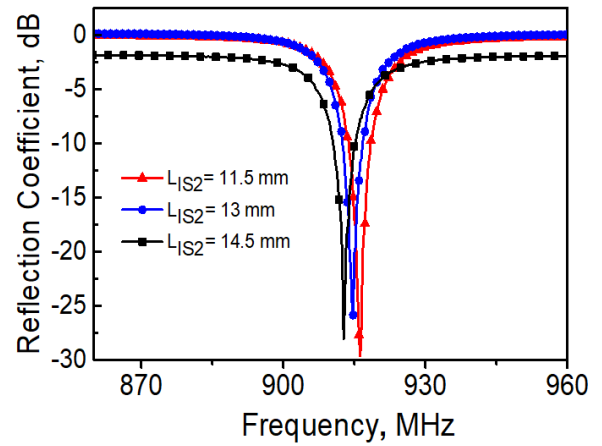
(c)

FIGURE 12. The impact on shorted inductive (w_s) to (a) The changes of input resistance and reactance. (b) Reflection coefficient (dB). (c) Power transmission coefficient across the different frequencies.

Next, the correlations among the small shorted inductive or the shorting wall, the resistance, and the reactance of the proposed antenna were studied. As shown in Fig. 12a, the small shorted inductive was first considered for the case of 0.8 mm $\leq W_s \leq$ 1.0 mm as the tag antenna operated at the

resonance frequency of 915 MHz. The input impedance of the tag antenna decreased rapidly from 25+280 Ω to 16.1+225 Ω when W_s was extended from 0.8 to 1.0 mm. By contrast, the input impedance of the proposed antenna did not change considerably when W_s was in the range of 1.4–1.8 mm. The resistance and reactance of the proposed antenna for the case of 1.0 mm $\leq W_s \leq$ 1.4 mm were observed to linearly decrease. The input resistance and reactance increased from 8.4 to 16.1 Ω and from 183.37 to 224.94 Ω, respectively, when W_s decreased from 1.4 to 1.0 mm. The input resistance and reactance were also found to decrease at a lower rate as W_s increase above 1.2 mm. This means that coarse tuning of the proposed antenna can be performed by combining the shorted inductive plate, I-slot 1, and open and closed slots. Notably, the performance of the proposed antenna with the reflection coefficient and power transmission coefficient (PTC) was almost unchanged in this scenario, as shown in Figs. 12b and 12c.
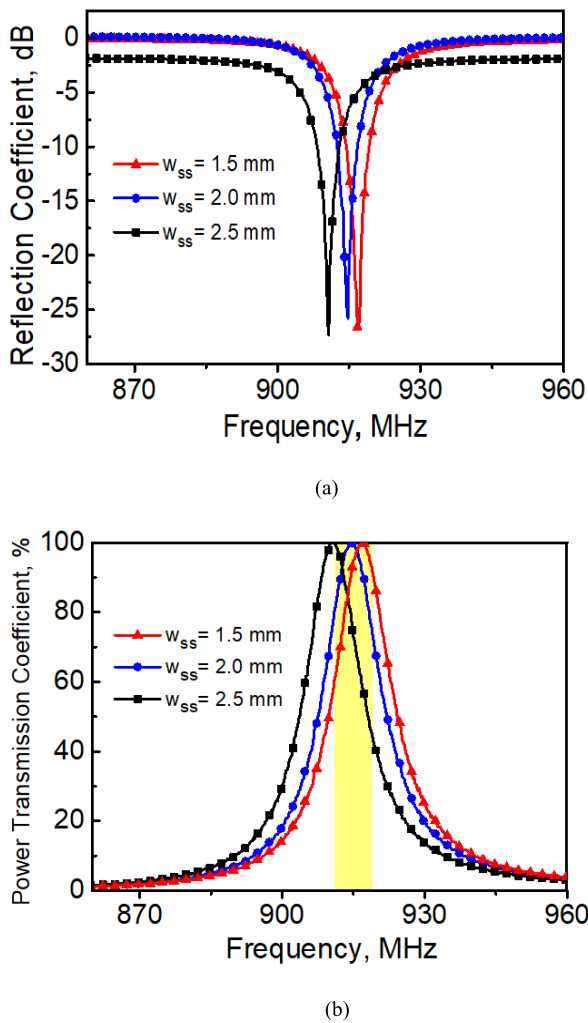
(a)

(b)

FIGURE 14. The impact on open slits (W_SS) to (a) The input impedance; (b) Reflection coefficient (dB). (c) Power transmission coefficient across the different frequencies.

Next, the effects of I-slot 2 ($L_{IS2} = 2L_{is} + V_{is}$) and open slits ($w_{SS}$) were evaluated (see Figs. 13 and 14). Varying the total length of L_{IS2} caused the proposed antenna's resonance frequency to shift substantially slowly at a rate of 1.5 MHz in 1.5 mm (see Fig. 13a) while maintaining an unchanged PTC of approximately 100% (see Fig. 13b).

Similarly, increasing the width of the total open slits (W_{SS}) in the range of 1.5–2.5 mm caused the tag's resonance frequency to shift slowly at a rate of 3 MHz in 0.5 mm increments (Fig. 14a). In addition, the power transmission coefficient remained unchanged as the width of the total open slits was increased by 0.5 mm. This was logical as the narrow open slits were less resistive and inductive than closed slots. Figs. 13 and 14 show that I-slot 2 and open slits were useful for fine-tuning the proposed antenna's resonance frequency.

Finally, the effects of changing the size of the backing metal were analyzed (Fig. 15). In [19] and [36], when the tags were mounted on or close to the metals, many problems arose. For example, the directivity pattern tended to increase,

the radiation efficiency decreased owing to the decreasing radiating resistance, and the tag's impedance changed statistical significance and caused a low power transmission coefficient. However, the proposed tag's structure achieved a favorable tradeoff between the increasing directivity and radiation efficiency, and the input impedance of the tag antenna did not change at the resonance frequency for the electrically small tag, thereby ensuring that the PTC was almost the same. Specifically, the resonance frequency was shifted very slowly at a rate of 3.0 MHz when the dimensions of the metallic plate varied greatly from 50×50 mm^2 to 250×250 mm^2 in 50 mm steps and increased slightly as the resonance frequency became greater than 923 MHz (see Fig. 15b). This is because the resistance and inductance of the tag antenna were less changed at 915 MHz, as shown in Fig. 15a. Furthermore, the directivity and radiation efficiency were enhanced significantly from 1.89 to 4.77 dB and from 11% to 22% (see Fig. 15d), respectively. The size change of the back metal also caused the proposed antenna to switch from having an omnidirectional pattern to having a desired directional pattern (see Fig. 15e). In all cases of the different backing metal sizes, the reflection coefficient values are always greater than 20 dB (approximates more than 99 % power transfer efficiency), as plotted in Fig. 15c.

In general, all parameter evaluations showed that the resonance frequency of the proposed antenna could be easily shifted to any frequencies in the bands for North and South America (860–960 and 902–928 MHz, respectively) through the control of coarse tuning (shorted inductive, I-slot 1, and open and closed slots) and fine-tuning (I-slot 2 and small open slits), and the PTC remained almost unchanged (∼100%). Further, the input impedance of the tag antenna was little sensitive to the change in the backing metal plate size, resulting in a high directivity pattern and radiation efficiency for a small tag.

VI. EXPERIMENT RESULTS AND DISCUSSION
The proposed antenna was fabricated by applying the three FR4 substrates (thickness: 0.8 mm for the radiating patch, 0.2 mm for the ground layer, and 0.4 mm for the shorted inductive on the side; dielectric constant $\varepsilon_r = 4.3$ and loss tangent $\delta = 0.025$) with the optimized design parameters listed in Table 1. The tag antenna must be conjugate-matched with the impedance of the UCODE8/8m chip, which has been measured to have a complex input impedance of $15 - j217$ Ω and minimum power sensitivity of -21.9 dBm at 915 MHz, as plotted in Fig. 4. To determine the input impedance of the proposed antenna, the measurement was performed using a balun probe applied through a cable with a characteristic impedance of 50 Ω, which was connected to the VNA. Notably, the balun probe was calibrated by ensuring it made contact with a short and load circuits on the calibration substrate before this measurement is performed (see Fig. 5). During the measurement process, the input impedance, reflection coefficient, power transmission coefficient, reading distance, and realized gain were determined when the tag antenna
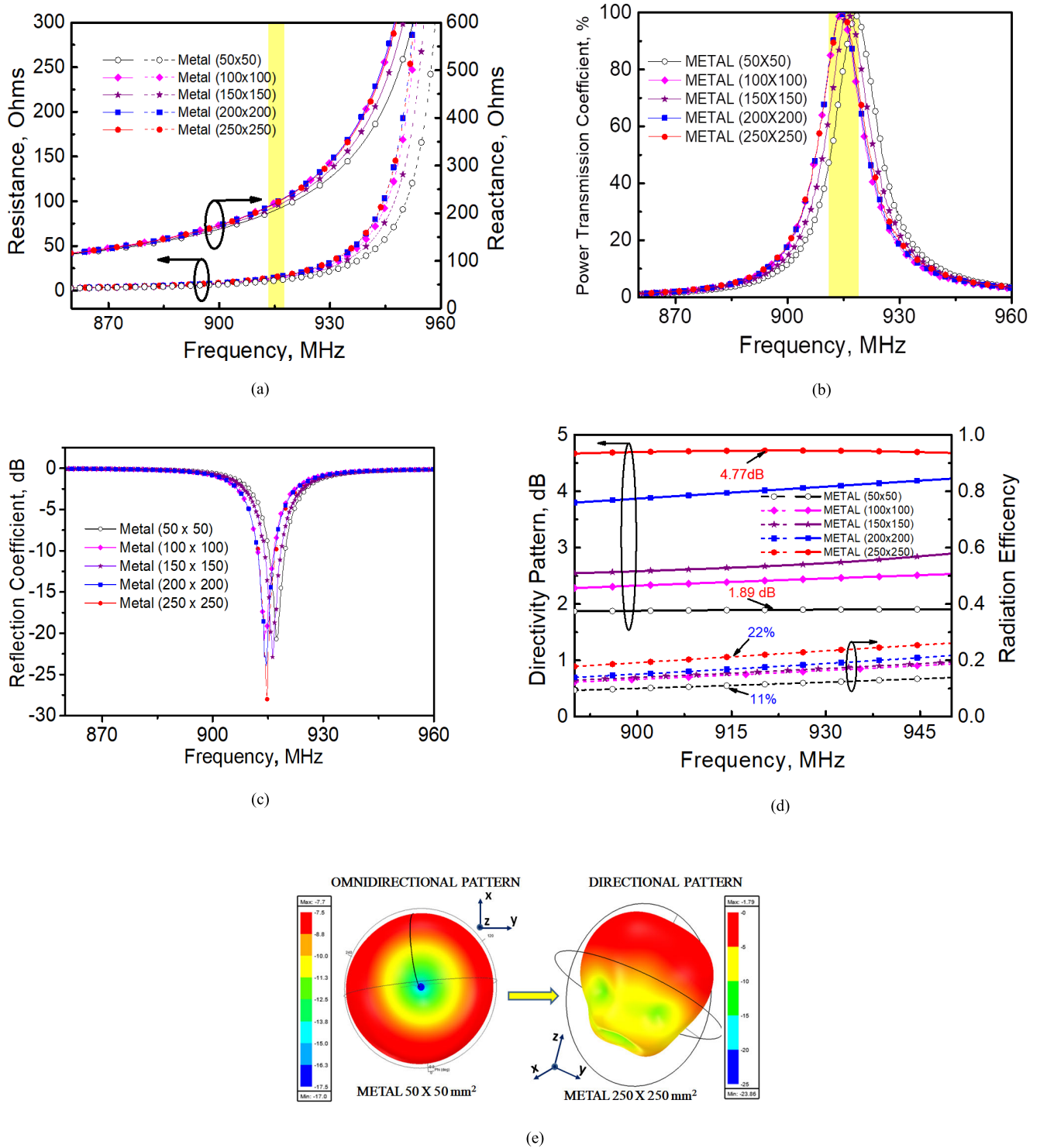
FIGURE 15. The impact on the backing metal sizes to (a) The input impedance. (b) Power transmission coefficient. (c) Reflection coefficient. (d) Directivity and radiation efficiency across the different frequencies; (e) The radiation patterns at 915 MHz.

was fixed in the middle of a metal object with optimal size of 250 mm × 250 mm and reinforced by a soft square foam plate (thickness: 1.0 mm) with relative permittivity of 1.03 (close to that of air), as shown in Fig. 3b. Under the optimized parameters given in Table 1, the results in Fig. 16 show that

the measured and simulated input impedances agreed well with the chip's impedance. Specifically, the tag antenna's measured and simulated complex impedance at a resonance frequency of 915 MHz were 16+j219 Ω and 14+j215 Ω, respectively.

FIGURE 16. The measurement and simulation impedances of the proposed antenna attached to a metal object with the size of 250 × 250 mm^2 compared to the chip's input impedance against the different frequencies.

FIGURE 17. The measurement and simulation reflection coefficient and power transmission coefficient of the proposed antenna attached to a metal object with the size of 250 × 250 mm^2.
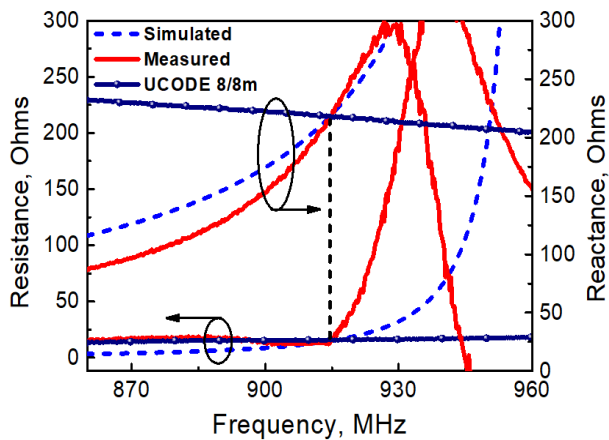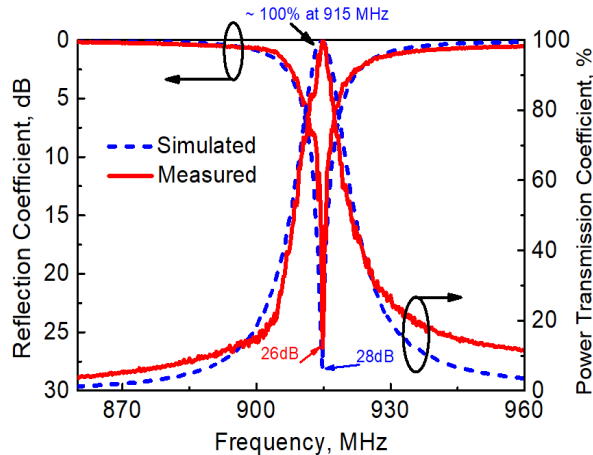
A slight shift was noted between the measured and simulated resistance and reactance values. This discrepancy was found from the deformation of the antenna structure when the flexible pins of the balun probe were attached to the pads during measurement. Further, the copper tape was used to short the radiating patch and the ground layer in this design, which also caused the resistance and reactance to vary.

Because the reflection coefficient (S_{11}) and power transmission coefficient (τ) cannot be instantly measured using the VNA, to validate the matching between the input impedance of the microchip and the proposed antenna, the following equation [37] was used for calculating the tag's characteristic performance parameters S_{11} and τ:

$$S_{11} = \frac{Z_{chip} - Z_{ant}^*}{Z_{chip} + Z_{ant}} \ (\dim ensionless), \ 0 \le |S_{11}| \le 1 \quad (2)$$

where $Z_{chip} = R_{chip} + jX_{chip}$ is the complex impedance of UCODE8/8m chip (X_{chip} is always negative) provided in the datasheet of the manufacturer, $Z_{ant} = R_{ant} + jX_{ant}$ is the complex antenna impedance (X_{ant} is always positive) determined through the simulation and measurement.

The reflection coefficient (unit: dB) is expressed as

$$S_{11}(dB) = -20 \log_{10} |S_{11}| \quad (3)$$

Then, the power transmission coefficient (τ) is given by

$$\begin{aligned} \tau &= \left(1 - |S_{11}|^2\right) \\ &= \frac{4R_{ant}R_{chip}}{\left(R_{ant} + R_{chip}\right)^2 + \left(X_{ant} + X_{chip}\right)^2} \end{aligned} \quad (4)$$

The measured and simulated reflection coefficient and power transmission coefficient are shown in Fig. 17, and the results indicate that the proposed antenna radiated best at 915 MHz, where the measured and simulated reflection coefficients were $|S_{11}| = 26$ dB and $|S_{11}| = 28$ dB, respectively. Both values were observed to be beyond 99% of the power

transmission coefficient that formed a conjugate pair, and the maximum power was transferred between the UCODE8/8m chip and the antenna. Furthermore, the measured and simulated bandwidths were found to be approximately 16 MHz (907–923 MHz) and 14 MHz (909–923 MHz), respectively. With this measured 3-dB impedance bandwidth of 1.42%, the range was not sufficient for covering the entire frequency band for North America (860–960 MHz). However, the range was almost sufficient for maintaining favorable operation in the frequency band for South America (902–928 MHz).

Realized gain (G_r) is another important parameter for evaluating tag performance. Realized gain (dB) can be easily determined from the product of the tag antenna gain and the impedance mismatch [38], [39] as follows:

$$G_r(\text{dB}) = G_{tag-ant} \ (\text{dB}).\tau \quad (5)$$

where $G_{tag-ant}$ is the gain of the tag antenna, τ is the power transmission coefficient which includes the result of impedance mismatch between the antenna and the UCODE chip.

Fig. 18 shows the measured and simulated gain of the proposed antenna mounted on the metallic plate of size 250 × 250 mm^2 from 850 MHz to 1 GHz. Good matching was indicated between the measured and simulated gains from 902–925 MHz with variable values of −6.54 dB to −5.5 dB; these cover almost the entire band for South America. At the desirable frequency of 915 MHz, the measured realized gain of the tag increased slightly to −2.3 dB, and the simulated gain was −1.8 dB. A small deviation of around 0.5 dB was observed between the measured and simulated results. This was because the chip impedance varied slightly when the pads were soldered at the excitation position in the antenna structure. The misalignment between the proposed antenna and the reader also contributed to these changes.

Finally, reading distance was among the most important parameters for deciding on the optimal RFID tag for various
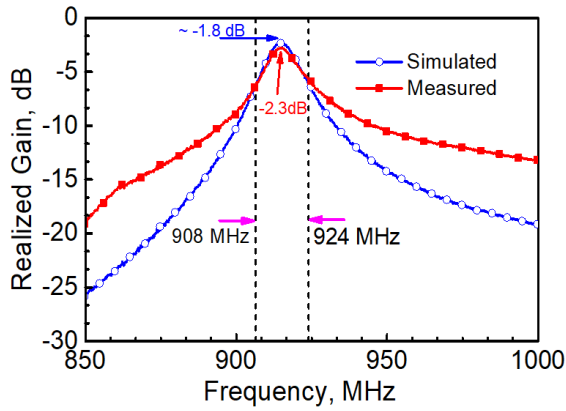
FIGURE 18. The measurement and simulation realized gains of the proposed antenna attached to a metal object with the size of 250 × 250 mm².
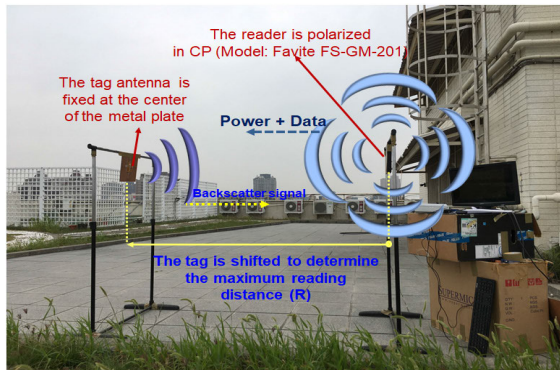

FIGURE 20. The reader and the tag antenna attached to a metal object with the size of 250 × 250 mm² are set up inside the chamber to observe the pattern sensitivity and reading distance.

root of both sides give the reading distance in the following simple form:

$$R = \frac{\lambda}{4\pi}\sqrt{\frac{P_{\text{reader-tx}}\, G_{\text{reader-ant}}\, G_{\text{tag-ant}}\, \chi\, \tau}{P_{\text{tag-chip}}}} \qquad (8)$$

From (8), the reading distance was the maximum when $P_{tag-chip}$ was equal to the minimum input power of the UCODE8/8m chip, $P_i(\min)$ (−21.9 dBm). Figs. 19 and 20 show the RFID system arrangement between the reader and the tag antenna for measuring the maximum reading distance in an open outdoor space. Further, the pattern sensitivity in a closed indoor environment was determined. The indoor and outdoor RFID tag measurement systems consist of a computer, a reader controller, and a CP reader antenna. The tag antenna was attached to the center of a metallic plate of size 250 × 250 mm². $R = 1$ m was the fixed distance between the reader and the tag antenna inside the chamber. However, R was shifted away from the reader antenna to determine the maximum reading distance in free space. Furthermore, the reader model used in this study is Favite FS-GF-801, which has a reader antenna gain of $G_{reader-ant} = 6$ dBi and a transmitter (T_X) output power of 30 dBm.

The measured input power pattern sensitivity of the proposed antenna is plotted in Fig. 21 in two planes under a condition wherein the tag is rotated around its axis in 15° increments. In the XZ plane, the minimum power sensitivity was observed at $\theta = 0°$ with power $P_{tag}(\min)$ of −12.5 dBm. The power sensitivity $P_{tag} \geq -8.6$ dBm was found at $-75° \leq \theta \leq 75°$, and the nulls ($P_{tag} = 0$ dBm) occurred for $\theta = \alpha$ (angular width $\alpha \approx 90°$). The values associated with (8) indicate that the maximum reading distance of the proposed antenna occurs when the incident direction of the wave of the reader antenna is parallel to the tag antenna at $\theta = 0°$, as shown in Fig. 21a. For a similar analysis in the YZ plane, the minimum power sensitivity was also obtained at $\theta = 0°$, with a power $P_{tag}(\min)$ of −15.2 dBm causing the

FIGURE 19. The reader and the tag antenna attached to a metal object with the size of 250 × 250 mm² are arranged in the free space to determine the maximum reading distance.

applications. In [40], the reading range of an RFID tag was determined using the free space Friis formula. First, the tag antenna receives energy from the reader antenna (see Fig. 19), as given by

$$P_{tag-ant} = \left(\frac{\lambda_o}{4\pi R}\right)^2 P_{reader-ant} G_{reader-ant} G_{tag-ant} \chi \quad (6)$$

where λ_0 is the wavelength in free space, $P_{tag-ant}$ is the power of the tag antenna, $P_{reader-ant}$ is the transmitted power from the reader antenna, $G_{reader-ant}$ is the gain of the reader antenna, $G_{tag-ant}$ is the gain of the tag antenna, and χ is the polarization matching coefficient between the tag antenna and the reader antenna.

In this scenario, the circularly polarized (CP) antenna is the reader antenna, and the tag antenna is horizontally or vertically polarized. Thus, χ will be 0.5 or −3 dB.

Then, the power received from the tag antenna was delivered to the UCODE chip; this power is expressed as

$$P_{tag-chip} = \tau . P_{tag-ant} \qquad (7)$$

where τ is the power transmission coefficient determined using (4). Now, substituting (7) into (6) and taking the square
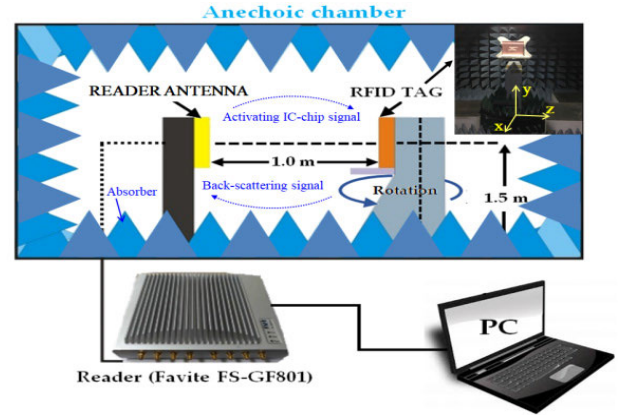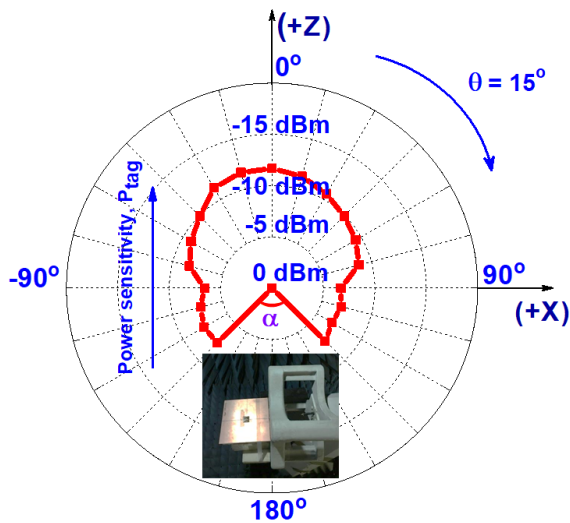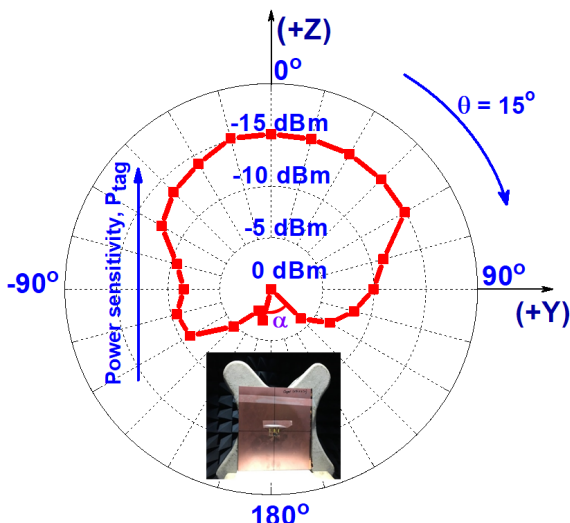
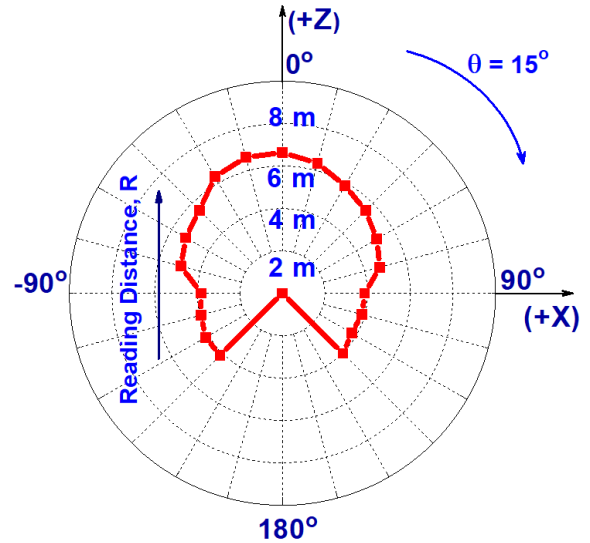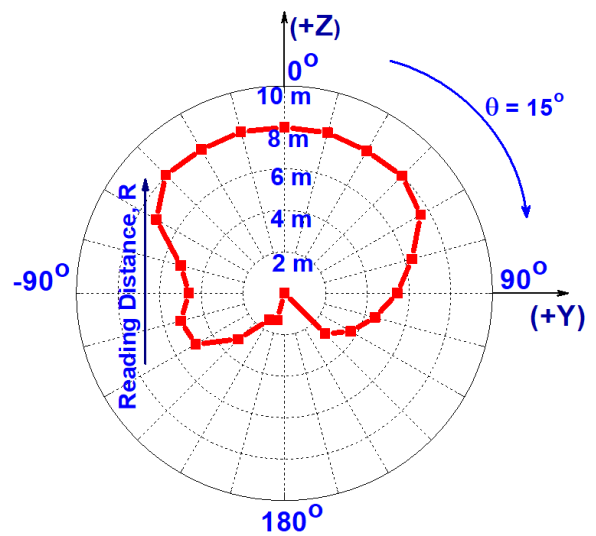**FIGURE 21.** The measured power sensitivity of the proposed antenna attached to a metal object with the size of 250 × 250 mm² with different angles in theta (θ) at 915 MHz in (a) XZ plane. (b) YZ plane.

FIGURE 22. The measured reading distance of the proposed antenna mounted on a metal object with the size of 250 × 250 mm² with different angles of theta (θ) at 915 MHz in (a) XZ plane. (b) YZ plane.

maximum distance between the tag antenna and the reader antenna or causing the incident direction of the wave of the reader antenna to aligned with the tag antenna surface at $\theta = 0°$. The power sensitivity $P_{tag} \geq -12.5$ dBm occurred at $-60° \leq \theta \leq 60°$, and the nulls ($P_{tag} = 0$ dBm) occurred for $\theta = \alpha$ ($\alpha \approx 60°$), as shown in Fig. 21b. Fig. 22 shows the maximum reading distance in the XZ and YZ planes. The reading distance was greater than 5 m for $-75° \leq \theta \leq 75°$, and it reached a maximum of 6.4 m for $\theta = 0°$ in the XZ plane (see Fig. 22a). In the YZ plane, for $-60° \leq \theta \leq 60°$, the reading distance was greater than 7 m, and the maximum distance was greater than 8.0 m for $\theta = 0°$ (see Fig. 22b). In general, the proposed antenna had a favorable broadside radiation pattern in both planes (covering an angular width

of $\theta \approx 150°$). Thus, it is a potential candidate for practical applications involving mounted on metallic objects.

Table 2 presents a comparison between the proposed tag antenna and recently reported tag antennas attached on a metallic surface. The tag antennas proposed in [9], [19], [16], [3] have smaller final dimensions than our model has. However, the realized gains of -12 dB and -16 dB in [3] and [16], respectively, were poor and resulted in much shorter maximum reading distances than our antenna had. The maximum reading distances were very long in [9] and [19]; however, these antennas have a three-layer structure. Although the tags in [2] and [5] had larger footprints than our tag had, they did not achieve better realized gain and reading distance. Further, these antennas

TABLE 2. The comparison of the performance characteristic parameters of the proposed antenna with the published works for a metal tag.

	Year	EIRP (W)	Number of layers	Chip threshold power (dBm)	Size of Tag (mm^3)	The volume of tag (mm^3)	Size of a backing metal (mm^2)	Realized gain (dB)	Radiation efficiency	Max. reading distance (m)	Fabrication Mechanism
This work		4	2	- 22.9	28.02 x 25.02 x 2.61	1820	250 x 250	-2.3	22%	8.1	Etched
[9]	2017	4	3	-20	23 x 16 x 1.6	588.8	200 x 200	-9	N/A	4.5	Folded + Etched
[19]	2014	4	3	-14	26 x 14 x 2.4	873.6	100 x 100	-1.4	23%	5.5	Etched
[16]	2013	4	3	-15	28 x 14 x 3.2	1254.4	200 x 200	-12	3%	1.8	Etched
[3]	2017	3.28	2	-20	31 x 31 x 1.6	1537.6	200 x 200	-16	N/A	1.8	Folded + Etched
[25]	2019	4	4	-20	25 x 25 x 3.2	2000	200 x 200	-0.78	40%	11	Folded + Etched
[5]	2020	4	3	-17.8	38 x 38 x 1.6	2310.4	200 x 200	-6.84	N/A	5.65	Folded + Etched
[2]	2018	3.28	3	-20	40 x 40 x 1.6	2560	200 x 200	-8	N/A	5	Folded + Etched
[20]	2020	4	2	-20	40 x 40 x 1.6	2560	200 x 200	-5.08	21.70%	7	Etched
[7]	2017	4	2	-17.8	30 x 30 x 3	2700	200 x 200	-5	N/A	7.2	Folded + Etched
[15]	2013	4	3	-15	56 x 26 x 3.2	4659.2	500 x 500	-4.8	N/A	4	Etched
[8]	2020	4	3	-20	45 x 45 x 3.2	6480	200 x 200	-1.57	73.80%	19	Folded + Etched
[31]	2016	4	2	-18	120 x 60 x 1.9	13680	150 x 300	8.7	> 80%	> 10	Etched

have a three-layer design with radiating aluminum plates, making it more difficult to achieve impedance matching with the microchip. The tag antenna developed in [25] achieved a higher realized gain of −0.78 dB and a radiation efficiency of 40; it also provided a long reading distance of 11 m. However, this antenna has a four-layer structure and uses the folded-patch technique. Such designs have a complex fabrication process and are more difficult to tune optimally. By using the same two layers as in our tag, the tags in [20] and [7] achieved a good reading distance (≥7 m); however, they these tags were larger than our one. The tag in [15] had a large impact on the backing metal dimension (500 × 500 mm^2), and therefore, it has a smaller maximum reading range and significantly larger size compared with our tag. The tags in [8] and [31] have large reading distances of more than 10 and 19 m, respectively, because these antennas were designed with an emphasis on gain and radiation efficiency. However, they have much larger dimensions (approximately 3.6 and 7.5 times larger, respectively) than our antenna has. Crucially, the designed antenna is easy to manufacture and has low threshold power sensitivity (−22.9 dBm).

VII. CONCLUSION
A compact antenna with flexible adjustment mechanisms was proposed and validated. Input impedance matching between the tag's antenna and an IC chip was easily achieved through the coarse tuning of the length of the shorted inductive, I-slot 1, and open and closed slots of I-shaped patches and through the fine-tuning of the width of I-slot 2 and two open slits. The proposed antenna, despite being electrically small, was unaffected by different sizes of backing metal objects and achieved reasonable gain and radiation efficiency. Furthermore, the tag prototype was inexpensive and could be fabricated through a simple method using FR4 substrates. The low-profile structure ($0.086\lambda_0 \times 0.076\lambda_0 \times 0.0079\lambda_0$) of this antenna afforded compactness. Moreover, this antenna achieved a high power transmission coefficient of 99.74% and a maximum reading distance of 8.1 m when mounted on a metallic plane of size 250×250 mm^2.

REFERENCES

[1] W.-H. Ng, E.-H. Lim, F.-L. Bong, and B.-K. Chung, "Folded patch antenna with tunable inductive slots and stubs for UHF tag design," *IEEE Trans. Antennas Propag.*, vol. 66, no. 6, pp. 2799–2806, Jun. 2018.

[2] N. M. Tan, H.-M. Chen, C.-Y.-D. Sim, and C.-H. Chen, "An inverted-F antenna for RFID tag mounted on a full container of liquid," in *Proc. IEEE Int. Symp. Antennas Propag. North Amer. Radio Sci. Meeting*, Montreal, QC, Canada, Jul. 2020, pp. 1523–1524.

[3] F.-L. Bong, E.-H. Lim, and F.-L. Lo, "Compact folded dipole with embedded matching loop for universal tag applications," *IEEE Trans. Antennas Propag.*, vol. 65, no. 5, pp. 2173–2181, May 2017.

[4] H.-D. Chen and Y.-H. Tsao, "Low-profile meandered patch antennas for RFID tags mountable on metallic objects," *IEEE Antennas Wireless Propag. Lett.*, vol. 9, pp. 118–121, 2010.

[5] S.-R. Lee, W.-H. Ng, E.-H. Lim, F.-L. Bong, and B.-K. Chung, "Compact magnetic loop antenna for omnidirectional on-metal UHF tag design," *IEEE Trans. Antennas Propag.*, vol. 68, no. 2, pp. 765–772, Feb. 2020.

[6] W.-H. Ng, E.-H. Lim, F.-L. Bong, and B.-K. Chung, "Compact planar Inverted-S antenna with embedded tuning arm for on-metal UHF RFID tag design," *IEEE Trans. Antennas Propag.*, vol. 67, no. 6, pp. 4247–4252, Jun. 2019.

[7] I.-Y. Park and D. Kim, "Artificial magnetic conductor loaded long-range passive RFID tag antenna mountable on metallic objects," *Electron. Lett.*, vol. 50, no. 5, pp. 335–336, Feb. 2014.

[8] R. C. Hadarig, M. E. de Cos, and F. Las-Heras, "UHF dipole-AMC combination for RFID applications," *IEEE Antennas Wireless Propag. Lett.*, vol. 12, pp. 1041–1044, 2013.

[9] R. C. Hadarig, M. E. de Cos Gomez, Y. Alvarez, and F. Las-Heras, "Novel bow-tie—AMC combination for 5.8-GHz RFID tags usable with metallic objects," *IEEE Antennas Wireless Propag. Lett.*, vol. 9, pp. 1217–1220, 2010.

[10] D. Kim and J. Yeo, "Dual-band long-range passive RFID tag antenna using an AMC ground plane," *IEEE Trans. Antennas Propag.*, vol. 60, no. 6, pp. 2620–2626, Jun. 2012.

[11] N. Ripin, E.-H. Lim, F.-L. Bong, and B.-K. Chung, "Miniature folded dipolar patch with embedded AMC for metal mountable tag design," *IEEE Trans. Antennas Propag.*, vol. 68, no. 5, pp. 3525–3533, May 2020.

[12] G. Marrocco, "The art of UHF RFID antenna design: Impedance-matching and size-reduction techniques," *IEEE Antennas Propag. Mag.*, vol. 50, no. 1, pp. 66–79, Feb. 2008.

[13] M. Hirvonen, P. Pursula, K. Jaakkola, and K. Laukkanen, "Planar inverted-F antenna for radio frequency identification," *Electron. Lett.*, vol. 40, no. 14, pp. 848–850, Jul. 2004.

[14] S.-L. Chen and K.-H. Lin, "A slim RFID tag antenna design for metallic object applications," *IEEE Antennas Wireless Propag. Lett.*, vol. 7, pp. 729–732, 2008.

[15] J. Zhang and Y. Long, "A dual-layer broadband compact UHF RFID tag antenna for platform tolerant application," *IEEE Trans. Antennas Propag.*, vol. 61, no. 9, pp. 4447–4455, Sep. 2013.

[16] J. Zhang and Y. Long, "A miniaturized via-patch loaded dual-layer RFID tag antenna for metallic object applications," *IEEE Antennas Wireless Propag. Lett.*, vol. 12, pp. 1184–1187, Sep. 2013.

[17] K. Jaakkola, "Small on-metal UHF RFID transponder with long read range," *IEEE Trans. Antennas Propag.*, vol. 64, no. 11, pp. 4859–4867, Nov. 2016.

[18] C. Y. Chiu, K. M. Shum, and C. H. Chan, "A tunable via-patch loaded PIFA with size reduction," *IEEE Trans. Antennas Propag.*, vol. 55, no. 1, pp. 65–71, Jan. 2007.

[19] J. Zhang and Y. Long, "A novel metal-mountable electrically small antenna for RFID tag applications with practical guidelines for the antenna design," *IEEE Trans. Antennas Propag.*, vol. 62, no. 11, pp. 5820–5829, Nov. 2014.

[20] Y.-H. Lee, E.-H. Lim, F.-L. Bong, and B.-K. Chung, "Loop-fed planar inverted-L antennas (PILAs) for omnidirectional UHF on-metal tag design," *IEEE Trans. Antennas Propag.*, vol. 68, no. 8, pp. 5864–5871, Aug. 2020.

[21] C.-W. Moh, E.-H. Lim, F.-L. Bong, and B.-K. Chung, "Miniature coplanar-fed folded patch for metal mountable UHF RFID tag," *IEEE Trans. Antennas Propag.*, vol. 66, no. 5, pp. 2245–2253, May 2018.

[22] W.-H. Ng, E.-H. Lim, F.-L. Bong, and B.-K. Chung, "E-shaped folded-patch antenna with multiple tuning parameters for on-metal UHF RFID tag," *IEEE Trans. Antennas Propag.*, vol. 67, no. 1, pp. 56–64, Jan. 2018.

[23] F.-L. Bong, E.-H. Lim, and F.-L. Lo, "Miniaturized dipolar patch antenna with narrow meandered slotline for UHF tag," *IEEE Trans. Antennas Propag.*, vol. 65, pp. 4435–4442, Sep. 2017.

[24] Y.-H. Lee, C.-W. Moh, E.-H. Lim, F.-L. Bong, and B.-K. Chung, "Miniature folded patch with differential coplanar feedline for metal mountable UHF RFID tag," *IEEE J. Radio Freq. Identificat.*, vol. 4, no. 2, pp. 93–100, Jun. 2020.

[25] N. M. Tan, Y.-F. Lin, C.-H. Chen, C.-H. Chang, Y.-C. Tseng, and H.-M. Chen, "Shorted patch antenna with tuning slit for RFID tag mounted on metallic plane," in *Proc. Int. Workshop Electromagn., Appl. Student Innov. Competition (iWEM)*, Penghu, Taiwan, Aug. 2020, pp. 1–2.

[26] Accessed: Sep. 10, 2019. [Online]. Available: https://www.ansys.com/blog/ansys-2019-r3-user-experience-and-autonomous-vehicle-development

[27] Accessed: Apr. 1, 2021. [Online]. Available: https://www.datasheets.com/en/search?q=FR4%2520PCB

[28] Accessed: Apr. 1, 2021. [Online]. Available: https://www.laird.com/sites/default/files/ds-eccostock-pp.pdf

[29] Accessed: Apr. 1, 2021. [Online]. Available: https://www.nxp.com/docs/en/data-sheet/SL3S1205-15-DS.pdf

[30] C.-H. Loo, K. Elmahgoub, F. Yang, A. Z. Elsherbeni, D. Kajfez, A. A. Kishk, T. Elsherbeni, L. Ukkonen, L. Sydanheimo, M. Kivikoski, S. Merilampi, and P. Ruuskanen, "Chip impedance matching for UHF RFID tag antenna design," *Prog. Electromagn. Res.*, vol. 81, pp. 359–370, 2008.

[31] Y. F. Lin, M. J. Chang, H. M. Chen, and B. Y. Lai, "Gain enhancement of ground radiation antenna for RFID tag mounted on metallic plane," *IEEE Trans. Antennas Propag.*, vol. 64, no. 4, pp. 1193–1200, Apr. 2016.

[32] A. Ghiotto, S. F. Cantalice, T. P. Vuong, A. Pouzin, G. Fontgalland, and S. Tedjini, "Miniaturized patch antenna for the radio frequency identification of metallic objects," in *IEEE MTT-S Int. Microw. Symp. Dig.*, Atlanta, GA, USA, Jun. 2008, pp. 583–586.

[33] A. Ria, A. Michel, R. K. Singh, V. Franchina, P. Bruschi, and P. Nepa, "Performance analysis of a compact UHF RFID ceramic tag in high-temperature environments," *IEEE J. Radio Freq. Identificat.*, vol. 4, no. 4, pp. 461–467, Dec. 2020.

[34] H. Li, J. Zhu, and Y. Yu, "Compact single-layer RFID tag antenna tolerant to background materials," *IEEE Access*, vol. 5, pp. 21070–21079, 2017.

[35] C. Pfeiffer, "Fundamental efficiency limits for small metallic antennas," *IEEE Trans. Antennas Propag.*, vol. 65, no. 4, pp. 1642–1650, Apr. 2017.

[36] S. R. Aroor and D. D. Deavours, "Evaluation of the state of passive UHF RFID: An experimental approach," *IEEE Systems J.*, vol. 1, no. 2, pp. 168–176, Nov. 2007.

[37] M. Nguyen, Y. Lin, C. Chang, C. Chen, and H. Chen, "Compact shorted C-shaped patch antenna for ultrahigh frequency radio frequency identification tags mounted on a metallic plate," *Int. J. RF Microw. Comput.-Aided Eng.*, vol. 31, no. 6, Jun. 2021, Art. no. e22595.

[38] Y. H. Lee, E. H. Lim, and F. L. Bong, "Compact folded C-shaped antenna for metal-mountable UHF RFID applications," *IEEE Trans. Antennas Propag.*, vol. 67, no. 2, pp. 765–773, Feb. 2018.

[39] P. V. Nikitin and K. V. S. Rao, "Gain measurement of antennas using RFID," in *Proc. IEEE Int. Symp. Antennas Propag. (APSURSI)*, Spokane, WA, USA, Jul. 2011, pp. 1012–1015.

[40] Z. N. Chen, *Antennas for Portable Devices*. Hoboken, NJ, USA: Wiley, 2007.

MINH-TAN NGUYEN received the B.S. degree in physics and the M.S. degree in electronics and telecommunication engineering from Vietnam National University Ho Chi Minh City, in 2007 and 2013, respectively. He is currently pursuing the Ph.D. degree in electronic engineering with the Institute of Photonics Engineering, National Kaohsiung University of Science and Technology. His main research interests include antenna design for RFID tags and MIMO antennas. Under the guidance of his advisor, he has been awarded the Best Student Paper Award in the 2020 IEEE International Workshop on Electromagnetics: Applications and Student Innovation Competition (IEEE IWEM 2020).

YI-FANG LIN received the B.S. degree in physics from the National Tsing Hua University, Hsinchu, Taiwan, in 1993, the M.S. degree from the Institute of Electro-Optical Engineering, National Sun Yat-sen University, Kaohsiung, Taiwan, in 1995, and the Ph.D. degree in electrical engineering from the National Sun Yat-sen University, in 1998. Since 2000, she has been with the Institute of Photonics Engineering, National Kaohsiung University of Science and Technology, Taiwan, where she became a Professor, in 2013. Her current research interests include microstrip antennas, dielectric resonator antennas, and small antennas design.

CHUN-HSIEN CHANG received the B.S. degree from the Department of Communication Engineering, National Penghu University of Science and Technology, in 2018, and the M.S. degree from the Institute of Photonics Engineering, National Kaohsiung University of Science and Technology, in 2021. His research interests include RFID antennas, beamforming antennas, and MIMO antennas.

HUA-MING CHEN (Senior Member, IEEE) received the B.S. degree in physics from the National Tsing Hua University, Hsinchu, Taiwan, in 1983, the M.S. degree from the Institute of Electro-Optics, National Chiao Tung University, Hsinchu, in 1987, and the Ph.D. degree in electrical engineering from the National Sun Yat-sen University, Kaohsiung, Taiwan, in 1996. Since 1988, he has been with the Institute of Photonics and Communications, National Kaohsiung University of Science and Technology, Kaohsiung, where he became a Professor, in 2001. He served as the Director for the Institute of Photonics and Communications, National Kaohsiung University of Science and Technology, from 2005 to 2008. He has published more than 110 journals and conference papers and takes out 20 patents on antenna design. Several of his antenna designs have been licensed to industry for production. His current research interests include antennas for smart connected devices, dielectric resonator antennas, RFID antennas, and microwave filter design. He was elected as the President of the Institute of Antennas Engineers of Taiwan (IAET), in 2010–2012. He has received the IEEE 2011 Best Chapter Award. He served as a Trustees for IEEE Tainan Section, from 2010 to 2011, and Chinese Microwave Association, from 2009 to 2011. He was elected as the Chair of IEEE AP-S Tainan Chapter, from 2009 to 2010. He served as a Publications Committee Chair for ISAP 2014, International Technical Program Committee Member of IEEE AEM2C 2010, and IEEE iWEM 2011 in Taiwan.

CHIEN-HUNG CHEN (Member, IEEE) received the B.S. degree in electronic engineering from R.O.C. Air Force Academy, Taiwan, in 2004, the M.S. degree from the Institute of Communication and Photonics, National Kaohsiung University of Science and Technology, Taiwan, in 2007, and the Ph.D. degree in electrical engineering from the National Kaohsiung University of Science and Technology, in 2012. He was a Visiting Professor with the University of Florida, in 2014. He is currently an Associate Professor and the Department Chairman of avionics at R.O.C. Air Force Academy. His research interests include avionics antennas and microwave system design. He has been an IEEE AP-S Tainan Chapter Vice Chairman, since 2017.

• • •